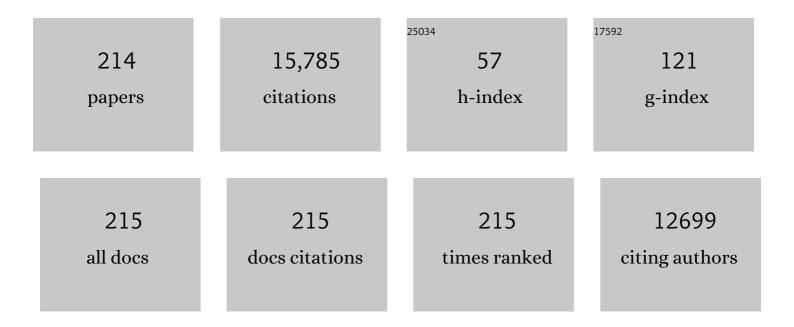
List of Publications by Year in descending order

Source: https://exaly.com/author-pdf/5505122/publications.pdf Version: 2024-02-01



IIN CHEN

#	Article	IF	CITATIONS
1	Correcting the Saturation Effect in DMSP/OLS Stable Nighttime Light Products Based on Radiance-Calibrated Data. IEEE Transactions on Geoscience and Remote Sensing, 2022, 60, 1-11.	6.3	3
2	An Automatic Processing Framework for <i>In Situ</i> Determination of Ecohydrological Root Water Content by Ground-Penetrating Radar. IEEE Transactions on Geoscience and Remote Sensing, 2022, 60, 1-15.	6.3	2
3	Tidal phenomenon of the dockless bike-sharing system and its causes: the case of Beijing. International Journal of Sustainable Transportation, 2022, 16, 287-300.	4.1	8
4	Enhanced Spatiotemporal Fusion via MODIS-Like Images. IEEE Transactions on Geoscience and Remote Sensing, 2022, 60, 1-17.	6.3	6
5	Snow cover detection in mid-latitude mountainous and polar regions using nighttime light data. Remote Sensing of Environment, 2022, 268, 112766.	11.0	15
6	Greater temperature sensitivity of vegetation greenup onset date in areas with weaker temperature seasonality across the Northern Hemisphere. Agricultural and Forest Meteorology, 2022, 313, 108759.	4.8	12
7	Understanding the Role of Receptive Field of Convolutional Neural Network for Cloud Detection in Landsat 8 OLI Imagery. IEEE Transactions on Geoscience and Remote Sensing, 2022, 60, 1-17.	6.3	6
8	Stacked spectral feature space patch: An advanced spectral representation for precise crop classification based on convolutional neural network. Crop Journal, 2022, 10, 1460-1469.	5.2	13
9	A novel framework to assess all-round performances of spatiotemporal fusion models. Remote Sensing of Environment, 2022, 274, 113002.	11.0	28
10	Fusing or filling: Which strategy can better reconstruct high-quality fine-resolution satellite time series?. Science of Remote Sensing, 2022, 5, 100046.	4.8	4
11	Detecting crop phenology from vegetation index time-series data by improved shape model fitting in each phenological stage. Remote Sensing of Environment, 2022, 277, 113060.	11.0	20
12	The FIRST model: Spatiotemporal fusion incorrporting spectral autocorrelation. Remote Sensing of Environment, 2022, 279, 113111.	11.0	12
13	Enhanced Spatial–Temporal Savitzky–Golay Method for Reconstructing High-Quality NDVI Time Series: Reduced Sensitivity to Quality Flags and Improved Computational Efficiency. IEEE Transactions on Geoscience and Remote Sensing, 2022, 60, 1-17.	6.3	3
14	Evaluation of Vegetation Indexes and Green-Up Date Extraction Methods on the Tibetan Plateau. Remote Sensing, 2022, 14, 3160.	4.0	6
15	Sensitivity of six typical spatiotemporal fusion methods to different influential factors: A comparative study for a normalized difference vegetation index time series reconstruction. Remote Sensing of Environment, 2021, 252, 112130.	11.0	76
16	Optimal Color Composition Method for Generating High-Quality Daily Photographic Time Series From PhenoCam. IEEE Journal of Selected Topics in Applied Earth Observations and Remote Sensing, 2021, 14, 6179-6193.	4.9	4
17	Adaptive Component Discrimination Network for Airplane Detection in Remote Sensing Images. IEEE Journal of Selected Topics in Applied Earth Observations and Remote Sensing, 2021, 14, 7699-7713.	4.9	8
18	Adopting "Difference-in-Differences―Method to Monitor Crop Response to Agrometeorological Hazards with Satellite Data: A Case Study of Dry-Hot Wind. Remote Sensing, 2021, 13, 482.	4.0	8

#	Article	IF	CITATIONS
19	GPR-Based Automatic Identification of Root Zones of Influence Using HDBSCAN. Remote Sensing, 2021, 13, 1227.	4.0	9
20	Forest Greening Increases Land Surface Albedo During the Main Growing Period Between 2002 and 2019 in China. Journal of Geophysical Research D: Atmospheres, 2021, 126, e2020JD033582.	3.3	11
21	Spatiotemporal fusion method to simultaneously generate full-length normalized difference vegetation index time series (SSFIT). International Journal of Applied Earth Observation and Geoinformation, 2021, 100, 102333.	2.8	19
22	A practical approach to reconstruct high-quality Landsat NDVI time-series data by gap filling and the Savitzky–Golay filter. ISPRS Journal of Photogrammetry and Remote Sensing, 2021, 180, 174-190.	11.1	89
23	Contextualizing human dynamics: Understanding the semantics of movement trajectories with Wi-Fi data. Travel Behaviour & Society, 2021, 25, 183-192.	5.0	6
24	The superiority of the normalized difference phenology index (NDPI) for estimating grassland aboveground fresh biomass. Remote Sensing of Environment, 2021, 264, 112578.	11.0	43
25	Improving the accuracy of spring phenology detection by optimally smoothing satellite vegetation index time series based on local cloud frequency. ISPRS Journal of Photogrammetry and Remote Sensing, 2021, 180, 29-44.	11.1	21
26	Graph Convolutional Networks-Based Super-Resolution Land Cover Mapping. IEEE Journal of Selected Topics in Applied Earth Observations and Remote Sensing, 2021, 14, 7667-7681.	4.9	10
27	Mapping a Paddy Rice Area in a Cloudy and Rainy Region Using Spatiotemporal Data Fusion and a Phenology-Based Algorithm. Remote Sensing, 2021, 13, 4400.	4.0	6
28	A geometric misregistration resistant data fusion approach for adding red-edge (RE) and short-wave infrared (SWIR) bands to high spatial resolution imagery. Science of Remote Sensing, 2021, 4, 100033.	4.8	8
29	A Supplementary Module to Improve Accuracy of the Quality Assessment Band in Landsat Cloud Images. Remote Sensing, 2021, 13, 4947.	4.0	3
30	Coarse-Resolution Satellite Images Overestimate Urbanization Effects on Vegetation Spring Phenology. Remote Sensing, 2020, 12, 117.	4.0	32
31	Response of winter wheat to spring frost from a remote sensing perspective: Damage estimation and influential factors. ISPRS Journal of Photogrammetry and Remote Sensing, 2020, 168, 221-235.	11.1	27
32	Thick cloud removal in Landsat images based on autoregression of Landsat time-series data. Remote Sensing of Environment, 2020, 249, 112001.	11.0	44
33	Remote Sensing Index for Mapping Canola Flowers Using MODIS Data. Remote Sensing, 2020, 12, 3912.	4.0	18
34	Comparison of MODIS-based vegetation indices and methods for winter wheat green-up date detection in Huanghuai region of China. Agricultural and Forest Meteorology, 2020, 288-289, 108019.	4.8	21
35	Does any phenological event defined by remote sensing deserve particular attention? An examination of spring phenology of winter wheat in Northern China. Ecological Indicators, 2020, 116, 106456.	6.3	23
36	Mapping global urban boundaries from the global artificial impervious area (GAIA) data. Environmental Research Letters, 2020, 15, 094044.	5.2	240

JIN CHEN

#	Article	IF	CITATIONS
37	Can changes in autumn phenology facilitate earlier green-up date of northern vegetation?. Agricultural and Forest Meteorology, 2020, 291, 108077.	4.8	36
38	A New Cross-Fusion Method to Automatically Determine the Optimal Input Image Pairs for NDVI Spatiotemporal Data Fusion. IEEE Transactions on Geoscience and Remote Sensing, 2020, 58, 5179-5194.	6.3	29
39	Mapping Winter Wheat in North China Using Sentinel 2A/B Data: A Method Based on Phenology-Time Weighted Dynamic Time Warping. Remote Sensing, 2020, 12, 1274.	4.0	46
40	Spatio-temporal fusion for remote sensing data: an overview and new benchmark. Science China Information Sciences, 2020, 63, 1.	4.3	74
41	A new sensor bias-driven spatio-temporal fusion model based on convolutional neural networks. Science China Information Sciences, 2020, 63, 1.	4.3	47
42	Mechanisms, monitoring and modeling of shrub encroachment into grassland: a review. International Journal of Digital Earth, 2019, 12, 625-641.	3.9	25
43	Potential effects of heat waves on the population dynamics of the dengue mosquito Aedes albopictus. PLoS Neglected Tropical Diseases, 2019, 13, e0007528.	3.0	24
44	How Does Scale Effect Influence Spring Vegetation Phenology Estimated from Satellite-Derived Vegetation Indexes?. Remote Sensing, 2019, 11, 2137.	4.0	25
45	A semi-analytical snow-free vegetation index for improving estimation of plant phenology in tundra and grassland ecosystems. Remote Sensing of Environment, 2019, 228, 31-44.	11.0	32
46	Measurement of blooming effect of DMSP-OLS nighttime light data based on NPP-VIIRS data. Annals of GIS, 2019, 25, 153-165.	3.1	14
47	A simple self-adjusting model for correcting the blooming effects in DMSP-OLS nighttime light images. Remote Sensing of Environment, 2019, 224, 401-411.	11.0	50
48	Replacing the Red Band with the Red-SWIR Band (0.74ïred+0.26ïswir) Can Reduce the Sensitivity of Vegetation Indices to Soil Background. Remote Sensing, 2019, 11, 851.	4.0	22
49	An Improved Flexible Spatiotemporal DAta Fusion (IFSDAF) method for producing high spatiotemporal resolution normalized difference vegetation index time series. Remote Sensing of Environment, 2019, 227, 74-89.	11.0	119
50	Comparison of Winter Wheat Spring Phenology Extraction by Various Remote Sensing Vegetation Indices and Methods. , 2019, , .		2
51	A Method to Improve the GCC Series of Phenology Cameras Based on Histogram Features Using Multiple Linear Regression. , 2019, , .		Ο
52	Quantitative Evaluation for the Blooming Effect of Nighttime Light Data in China. , 2019, , .		0
53	An Object-Based Strategy for Improving the Accuracy of Spatiotemporal Satellite Imagery Fusion for Vegetation-Mapping Applications. Remote Sensing, 2019, 11, 2927.	4.0	9
54	Assessing the impact of endmember variability on linear Spectral Mixture Analysis (LSMA): A theoretical and simulation analysis. Remote Sensing of Environment, 2019, 235, 111471.	11.0	33

#	Article	IF	CITATIONS
55	Correlation between Root Density and Soil Moisture of Caragana Microphylla in Xilinhot Grassland. , 2019, , .		0
56	Analysis of Topographic Effects on Vegetation Indices. , 2019, , .		0
57	Non-invasive estimation of root zone soil moisture from coarse root reflections in ground-penetrating radar images. Plant and Soil, 2019, 436, 623-639.	3.7	26
58	Measurement of soil water content using ground-penetrating radar: a review of current methods. International Journal of Digital Earth, 2019, 12, 95-118.	3.9	37
59	Detection of Root Orientation Using Ground-Penetrating Radar. IEEE Transactions on Geoscience and Remote Sensing, 2018, 56, 93-104.	6.3	22
60	Modeling vegetation green-up dates across the Tibetan Plateau by including both seasonal and daily temperature and precipitation. Agricultural and Forest Meteorology, 2018, 249, 176-186.	4.8	50
61	The mixed pixel effect in land surface phenology: A simulation study. Remote Sensing of Environment, 2018, 211, 338-344.	11.0	89
62	A new index for mapping the â€~blue steel tile' roof dominated industrial zone from Landsat imagery. Remote Sensing Letters, 2018, 9, 578-586.	1.4	8
63	A Novel Method for Removing Snow Melting-Induced Fluctuation in GIMMS NDVI3g Data for Vegetation Phenology Monitoring: A Case Study in Deciduous Forests of North America. IEEE Journal of Selected Topics in Applied Earth Observations and Remote Sensing, 2018, 11, 800-807.	4.9	11
64	"Blend-then-Index" or "Index-then-Blend": A Theoretical Analysis for Generating High-resolution NDVI Time Series by STARFM. Photogrammetric Engineering and Remote Sensing, 2018, 84, 65-73.	0.6	29
65	GlobeLand30: Operational global land cover mapping and big-data analysis. Science China Earth Sciences, 2018, 61, 1533-1534.	5.2	40
66	Mismatch in elevational shifts between satellite observed vegetation greenness and temperature isolines during 2000–2016 on the Tibetan Plateau. Global Change Biology, 2018, 24, 5411-5425.	9.5	60
67	A Novel Cloud Removal Method Based on IHOT and the Cloud Trajectories for Landsat Imagery. Remote Sensing, 2018, 10, 1040.	4.0	9
68	Estimating the age and population structure of encroaching shrubs in arid/semiarid grasslands using high spatial resolution remote sensing imagery. Remote Sensing of Environment, 2018, 216, 572-585.	11.0	22
69	A simple method to improve the quality of NDVI time-series data by integrating spatiotemporal information with the Savitzky-Golay filter. Remote Sensing of Environment, 2018, 217, 244-257.	11.0	172
70	A practical sampling method for assessing accuracy of detected land cover/land use change: Theoretical analysis and simulation experiments. ISPRS Journal of Photogrammetry and Remote Sensing, 2018, 144, 379-389.	11.1	5
71	An Automatic System for Reconstructing High-Quality Seasonal Landsat Time Series. , 2018, , 25-42.		7
72	Multiscale Integration Approach for Land Cover Classification Based on Minimal Entropy of Posterior Probability. IEEE Journal of Selected Topics in Applied Earth Observations and Remote Sensing, 2017, 10, 1105-1116.	4.9	11

#	Article	IF	CITATIONS
73	An Orthogonal Fisher Transformation-Based Unmixing Method Toward Estimating Fractional Vegetation Cover in Semiarid Areas. IEEE Geoscience and Remote Sensing Letters, 2017, 14, 449-453.	3.1	10
74	A snow-free vegetation index for improved monitoring of vegetation spring green-up date in deciduous ecosystems. Remote Sensing of Environment, 2017, 196, 1-12.	11.0	102
75	Mapping plastic greenhouse with medium spatial resolution satellite data: Development of a new spectral index. ISPRS Journal of Photogrammetry and Remote Sensing, 2017, 128, 47-60.	11.1	97
76	How does the dengue vector mosquito Aedes albopictus respond to global warming?. Parasites and Vectors, 2017, 10, 140.	2.5	34
77	Asymmetric Responses of the End of Growing Season to Daily Maximum and Minimum Temperatures on the Tibetan Plateau. Journal of Geophysical Research D: Atmospheres, 2017, 122, 13,278.	3.3	45
78	Identification of weather variables sensitive to dysentery in disease-affected county of China. Science of the Total Environment, 2017, 575, 956-962.	8.0	19
79	Remote Sensing Modelling and Parameter Inversion. Springer Geography, 2017, , 323-338.	0.4	0
80	Modeling Aboveground Biomass in Hulunber Grassland Ecosystem by Using Unmanned Aerial Vehicle Discrete Lidar. Sensors, 2017, 17, 180.	3.8	64
81	Exploring Determinants of Housing Prices in Beijing: An Enhanced Hedonic Regression with Open Access POI Data. ISPRS International Journal of Geo-Information, 2017, 6, 358.	2.9	47
82	Tree Root Automatic Recognition in Ground Penetrating Radar Profiles Based on Randomized Hough Transform. Remote Sensing, 2016, 8, 430.	4.0	56
83	Plant phenological synchrony increases under rapid within-spring warming. Scientific Reports, 2016, 6, 25460.	3.3	26
84	Global Land Surface Water Mapping and Analysis at 30 m Spatial Resolution for Years 2000 and 2010. Remote Sensing and Digital Image Processing, 2016, , 373-389.	0.7	3
85	Automated extraction of image-based endmember bundles of impervious layer using iterative classification strategy. , 2016, , .		0
86	Global cultivated land mapping at 30 m spatial resolution. Science China Earth Sciences, 2016, 59, 2275-2284.	5.2	28
87	Method for land cover classification accuracy assessment considering edges. Science China Earth Sciences, 2016, 59, 2318-2327.	5.2	5
88	A method characterizing urban expansion based on land cover map at 30 m resolution. Science China Earth Sciences, 2016, 59, 1738-1744.	5.2	12
89	Analysis for the spatial and temporal patterns of plasticulture in Shandong province, China with remotely sensed data. , 2016, , .		3
90	Effect of training strategy for positive and unlabelled learning classification: test on Landsat imagery. Remote Sensing Letters, 2016, 7, 1063-1072.	1.4	14

#	Article	IF	CITATIONS
91	A novel cloud removal method based on IHOT. , 2016, , .		1
92	A climate-driven mechanistic population model of Aedes albopictus with diapause. Parasites and Vectors, 2016, 9, 175.	2.5	42
93	Clobal mapping of artificial surfaces at 30-m resolution. Science China Earth Sciences, 2016, 59, 2295-2306.	5.2	25
94	Two-Step Constrained Nonlinear Spectral Mixture Analysis Method for Mitigating the Collinearity Effect. IEEE Transactions on Geoscience and Remote Sensing, 2016, 54, 2873-2886.	6.3	14
95	A Simple Method for Detecting Phenological Change From Time Series of Vegetation Index. IEEE Transactions on Geoscience and Remote Sensing, 2016, 54, 3436-3449.	6.3	29
96	An Iterative Haze Optimized Transformation for Automatic Cloud/Haze Detection of Landsat Imagery. IEEE Transactions on Geoscience and Remote Sensing, 2016, 54, 2682-2694.	6.3	49
97	A flexible spatiotemporal method for fusing satellite images with different resolutions. Remote Sensing of Environment, 2016, 172, 165-177.	11.0	461
98	Clobal cultivated land mapping at 30 m spatial resolution: Alias DOI. Science China Earth Sciences, 2016, 59, 2275-2284.	5.2	0
99	Identification of climate factors related to human infection with avian influenza A H7N9 and H5N1 viruses in China. Scientific Reports, 2015, 5, 18094.	3.3	33
100	A quantitative assessment of multiple scattering in plant-soil mixtures and the implications on nonlinear spectral unmixing models. , 2015, , .		0
101	A Method for Screening Climate Change-Sensitive Infectious Diseases. International Journal of Environmental Research and Public Health, 2015, 12, 767-783.	2.6	20
102	An Improved Method for Producing High Spatial-Resolution NDVI Time Series Datasets with Multi-Temporal MODIS NDVI Data and Landsat TM/ETM+ Images. Remote Sensing, 2015, 7, 7865-7891.	4.0	103
103	Intraspecific root competition of Caragana microphylla dominates its above-ground population self-thinning: Evidences from GPR. , 2015, , .		0
104	Effect of training strategy on PUL-SVM classification for cropland mapping by Landsat imagery. , 2015, , \cdot		1
105	An improved automated land cover updating approach by integrating with downscaled NDVI time series data. Remote Sensing Letters, 2015, 6, 29-38.	1.4	26
106	Calibrating the impact of root orientation on root quantification using ground-penetrating radar. Plant and Soil, 2015, 395, 289-305.	3.7	31
107	Mapping Grassland Wildfire Risk of the World. IHDP/Future Earth-integrated Risk Governance Project Series, 2015, , 277-283.	0.8	6
108	Assessment of Multiple Scattering in the Reflectance of Semiarid Shrublands. IEEE Transactions on Geoscience and Remote Sensing, 2015, 53, 4910-4921.	6.3	14

#	Article	IF	CITATIONS
109	A Modified Semianalytical Algorithm for Remotely Estimating Euphotic Zone Depth in Turbid Inland Waters. IEEE Journal of Selected Topics in Applied Earth Observations and Remote Sensing, 2015, 8, 1545-1554.	4.9	7
110	Logistical routing of park tours with waiting times: case of Beijing Zoo. Tourism Geographies, 2015, 17, 208-222.	4.0	9
111	Estimation of Fractional Vegetation Cover in Semiarid Areas by Integrating Endmember Reflectance Purification Into Nonlinear Spectral Mixture Analysis. IEEE Geoscience and Remote Sensing Letters, 2015, 12, 1175-1179.	3.1	19
112	Global land cover mapping at 30m resolution: A POK-based operational approach. ISPRS Journal of Photogrammetry and Remote Sensing, 2015, 103, 7-27.	11.1	1,301
113	Temperature sensitivity of spring vegetation phenology correlates to within-spring warming speed over the Northern Hemisphere. Ecological Indicators, 2015, 50, 62-68.	6.3	76
114	Spatiotemporal reflectance blending in a wetland environment. International Journal of Digital Earth, 2015, 8, 364-382.	3.9	12
115	An improved logistic method for detecting spring vegetation phenology in grasslands from MODIS EVI time-series data. Agricultural and Forest Meteorology, 2015, 200, 9-20.	4.8	106
116	Earlier-Season Vegetation Has Greater Temperature Sensitivity of Spring Phenology in Northern Hemisphere. PLoS ONE, 2014, 9, e88178.	2.5	98
117	The Estimation of Regional Crop Yield Using Ensemble-Based Four-Dimensional Variational Data Assimilation. Remote Sensing, 2014, 6, 2664-2681.	4.0	19
118	A Combination of TsHARP and Thin Plate Spline Interpolation for Spatial Sharpening of Thermal Imagery. Remote Sensing, 2014, 6, 2845-2863.	4.0	57
119	Changing Urban Form and Transport CO2 Emissions: An Empirical Analysis of Beijing, China. Sustainability, 2014, 6, 4558-4579.	3.2	40
120	Preliminary analysis of spatiotemporal pattern of global land surface water. Science China Earth Sciences, 2014, 57, 2330-2339.	5.2	23
121	High-resolution remote sensing mapping of global land water. Science China Earth Sciences, 2014, 57, 2305-2316.	5.2	69
122	Two new hyperspectral indices for comparing vegetation chlorophyll content. Geo-Spatial Information Science, 2014, 17, 17-25.	5.3	11
123	Subsurface lateral preferential flow network revealed by timeâ€lapse groundâ€penetrating radar in a hillslope. Water Resources Research, 2014, 50, 9127-9147.	4.2	77
124	Application of Crop Model Data Assimilation With a Particle Filter for Estimating Regional Winter Wheat Yields. IEEE Journal of Selected Topics in Applied Earth Observations and Remote Sensing, 2014, 7, 4422-4431.	4.9	60
125	Normalized difference vegetation index dynamic and spatiotemporal distribution of migratory birds in the Poyang Lake wetland, China. Ecological Indicators, 2014, 47, 219-230.	6.3	57
126	Spatialization of electricity consumption of China using saturation-corrected DMSP-OLS data. International Journal of Applied Earth Observation and Geoinformation, 2014, 28, 193-200.	2.8	81

#	Article	IF	CITATIONS
127	Can EVI-derived land-surface phenology be used as a surrogate for phenology of canopy photosynthesis?. International Journal of Remote Sensing, 2014, 35, 1162-1174.	2.9	52
128	Empirical comparison of noise reduction techniques for NDVI time-series based on a new measure. ISPRS Journal of Photogrammetry and Remote Sensing, 2014, 91, 17-28.	11.1	32
129	Restoration of Information Obscured by Mountainous Shadows Through Landsat TM/ETM+ Images Without the Use of DEM Data: A New Method. IEEE Transactions on Geoscience and Remote Sensing, 2014, 52, 313-328.	6.3	16
130	A simple error estimation method for linear-regression-based thermal sharpening techniques with the consideration of scale difference. Geo-Spatial Information Science, 2014, 17, 54-59.	5.3	10
131	Application of a Semianalytical Algorithm to Remotely Estimate Diffuse Attenuation Coefficient in Turbid Inland Waters. IEEE Geoscience and Remote Sensing Letters, 2014, 11, 1046-1050.	3.1	18
132	A simple method to simulate diurnal courses of PAR absorbed by grassy canopy. Ecological Indicators, 2014, 46, 129-137.	6.3	9
133	Comment on: "root orientation can affect detection accuracy of ground-penetrating radar― Plant and Soil, 2014, 380, 441-444.	3.7	9
134	Ground-penetrating radar-based automatic reconstruction of three-dimensional coarse root system architecture. Plant and Soil, 2014, 383, 155-172.	3.7	49
135	Earlier vegetation green-up has reduced spring dust storms. Scientific Reports, 2014, 4, 6749.	3.3	56
136	Forward simulation of root's ground penetrating radar signal: simulator development and validation. Plant and Soil, 2013, 372, 487-505.	3.7	22
137	Impact of root water content on root biomass estimation using ground penetrating radar: evidence from forward simulations and field controlled experiments. Plant and Soil, 2013, 371, 503-520.	3.7	59
138	Estimating Tree-Root Biomass in Different Depths Using Ground-Penetrating Radar: Evidence from a Controlled Experiment. IEEE Transactions on Geoscience and Remote Sensing, 2013, 51, 3410-3423.	6.3	39
139	A spectral gradient difference based approach for land cover change detection. ISPRS Journal of Photogrammetry and Remote Sensing, 2013, 85, 1-12.	11.1	70
140	An inherent limitation of solar-induced chlorophyll fluorescence retrieval at the O2-A absorption feature in high-altitude areas. IEEE Geoscience and Remote Sensing Letters, 2013, 10, 1567-1571.	3.1	2
141	Finer resolution observation and monitoring of global land cover: first mapping results with Landsat TM and ETM+ data. International Journal of Remote Sensing, 2013, 34, 2607-2654.	2.9	1,263
142	Retrieval of Inherent Optical Properties for Turbid Inland Waters From Remote-Sensing Reflectance. IEEE Transactions on Geoscience and Remote Sensing, 2013, 51, 3761-3773.	6.3	74
143	Two important indicators with potential to identify Caragana microphylla in xilin gol grassland from temporal MODIS data. Ecological Indicators, 2013, 34, 520-527.	6.3	17
144	The temporal hierarchy of shelters: a hierarchical location model for earthquake-shelter planning. International Journal of Geographical Information Science, 2013, 27, 1612-1630.	4.8	78

#	Article	IF	CITATIONS
145	Comparison of automatic thresholding methods for snow-cover mapping using Landsat TM imagery. International Journal of Remote Sensing, 2013, 34, 6529-6538.	2.9	42
146	Application of ground penetrating radar for coarse root detection and quantification: a review. Plant and Soil, 2013, 362, 1-23.	3.7	141
147	Quantitative assessment of the different methods addressing the endmember variability. , 2013, , .		2
148	Evaluation of wildfire propagation susceptibility in grasslands using burned areas and multivariate logistic regression. International Journal of Remote Sensing, 2013, 34, 6679-6700.	2.9	19
149	Atmospheric correction of ENVISAT/MERIS data over case II waters: the use of black pixel assumption in oxygen and water vapour absorption bands. International Journal of Remote Sensing, 2012, 33, 3713-3732.	2.9	1
150	A Framework for Supervised Image Classification with Incomplete Training Samples. Photogrammetric Engineering and Remote Sensing, 2012, 78, 595-604.	0.6	19
151	Scale Effect of Vegetation-Index-Based Spatial Sharpening for Thermal Imagery: A Simulation Study by ASTER Data. IEEE Geoscience and Remote Sensing Letters, 2012, 9, 549-553.	3.1	27
152	Specification of thermal growing season in temperate China from 1960 to 2009. Climatic Change, 2012, 114, 783-798.	3.6	38
153	Soft image segmentation model. , 2012, , .		2
154	Weighted misclassification rate: a new measure of classification error designed for landscape pattern index. Remote Sensing Letters, 2012, 3, 57-65.	1.4	4
155	A new geostatistical approach for filling gaps in Landsat ETM+ SLC-off images. Remote Sensing of Environment, 2012, 124, 49-60.	11.0	145
156	Comparison and improvement of methods for identifying waterbodies in remotely sensed imagery. International Journal of Remote Sensing, 2012, 33, 6854-6875.	2.9	158
157	An automated approach for updating land cover maps based on integrated change detection and classification methods. ISPRS Journal of Photogrammetry and Remote Sensing, 2012, 71, 86-95.	11.1	113
158	Mapping impervious surface expansion using medium-resolution satellite image time series: a case study in the Yangtze River Delta, China. International Journal of Remote Sensing, 2012, 33, 7609-7628.	2.9	88
159	A model for evacuation risk assessment with consideration of pre- and post-disaster factors. Computers, Environment and Urban Systems, 2012, 36, 207-217.	7.1	71
160	A Modified Neighborhood Similar Pixel Interpolator Approach for Removing Thick Clouds in Landsat Images. IEEE Geoscience and Remote Sensing Letters, 2012, 9, 521-525.	3.1	128
161	Influences of temperature and precipitation before the growing season on spring phenology in grasslands of the central and eastern Qinghai-Tibetan Plateau. Agricultural and Forest Meteorology, 2011, 151, 1711-1722.	4.8	345
162	Change Vector Analysis in Posterior Probability Space: A New Method for Land Cover Change Detection. IEEE Geoscience and Remote Sensing Letters, 2011, 8, 317-321.	3.1	105

#	Article	IF	CITATIONS
163	A Quantitative Analysis of Virtual Endmembers' Increased Impact on the Collinearity Effect in Spectral Unmixing. IEEE Transactions on Geoscience and Remote Sensing, 2011, 49, 2945-2956.	6.3	78
164	A Relaxed Matrix Inversion Method for Retrieving Water Constituent Concentrations in Case II Waters: The Case of Lake Kasumigaura, Japan. IEEE Transactions on Geoscience and Remote Sensing, 2011, 49, 3381-3392.	6.3	15
165	Modeling tree root diameter and biomass by ground-penetrating radar. Science China Earth Sciences, 2011, 54, 711-719.	5.2	62
166	A simple and effective method for filling gaps in Landsat ETM+ SLC-off images. Remote Sensing of Environment, 2011, 115, 1053-1064.	11.0	395
167	Estimating constituent concentrations in case II waters from MERIS satellite data by semi-analytical model optimizing and look-up tables. Remote Sensing of Environment, 2011, 115, 1247-1259.	11.0	75
168	Scale effect of vegetation index based thermal sharpening: A simulation study based on aster data. , 2011, , .		1
169	Practical image fusion method based on spectral mixture analysis. Science China Information Sciences, 2010, 53, 1277-1286.	4.3	6
170	An evacuation risk assessment model for emergency traffic with consideration of urban hazard installations. Science Bulletin, 2010, 55, 1000-1006.	1.7	10
171	An Enhanced Three-Band Index for Estimating Chlorophyll-a in Turbid Case-II Waters: Case Studies of Lake Kasumigaura, Japan, and Lake Dianchi, China. IEEE Geoscience and Remote Sensing Letters, 2010, 7, 655-659.	3.1	65
172	An enhanced spatial and temporal adaptive reflectance fusion model for complex heterogeneous regions. Remote Sensing of Environment, 2010, 114, 2610-2623.	11.0	929
173	Consistency of accuracy assessment indices for soft classification: Simulation analysis. ISPRS Journal of Photogrammetry and Remote Sensing, 2010, 65, 156-164.	11.1	20
174	Do flowers affect biomass estimate accuracy from NDVI and EVI?. International Journal of Remote Sensing, 2010, 31, 2139-2149.	2.9	43
175	Impact of collinearity on linear and nonlinear spectral mixture analysis. , 2010, , .		5
176	Quantifying the cool island intensity of urban parks using ASTER and IKONOS data. Landscape and Urban Planning, 2010, 96, 224-231.	7.5	423
177	Developing a MODIS-based index to discriminate dead fuel from photosynthetic vegetation and soil background in the Asian steppe area. International Journal of Remote Sensing, 2010, 31, 1589-1604.	2.9	61
178	Testing the spectral decomposition algorithm (SDA) for different phytoplankton species by a simulation based on tank experiments. International Journal of Remote Sensing, 2010, 31, 1605-1623.	2.9	9
179	NEW ALGORITHM FOR SPECTRAL MIXTURE ANALYSIS BASED ON FISHER DISCRIMINANT ANALYSIS: EVIDENCE FROM LABORATORY EXPERIMENT. Hongwai Yu Haomibo Xuebao/Journal of Infrared and Millimeter Waves, 2010, 28, 476-480.	0.2	0
180	Modelling the population density of China at the pixel level based on DMSP/OLS nonâ€radianceâ€calibrated nightâ€time light images. International Journal of Remote Sensing, 2009, 30, 1003-1018.	2.9	173

#	Article	IF	CITATIONS
181	Diurnal and seasonal variations in light-use efficiency in an alpine meadow ecosystem: causes and implications for remote sensing. Journal of Plant Ecology, 2009, 2, 173-185.	2.3	28
182	Yellow flowers can decrease NDVI and EVI values: evidence from a field experiment in an alpine meadow. Canadian Journal of Remote Sensing, 2009, 35, 99-106.	2.4	44
183	Land cover change detection with a cross orrelogram spectral matching algorithm. International Journal of Remote Sensing, 2009, 30, 3259-3273.	2.9	35
184	A SVM-based method to extract urban areas from DMSP-OLS and SPOT VGT data. Remote Sensing of Environment, 2009, 113, 2205-2209.	11.0	241
185	Location optimization algorithm for emergency signs in public facilities and its application to a single-floor supermarket. Fire Safety Journal, 2009, 44, 113-120.	3.1	32
186	Indicator of flower status derived from in situ hyperspectral measurement in an alpine meadow on the Tibetan Plateau. Ecological Indicators, 2009, 9, 818-823.	6.3	38
187	An automatic method for burn scar mapping using support vector machines. International Journal of Remote Sensing, 2009, 30, 577-594.	2.9	56
188	Estimating aboveground biomass of grassland having a high canopy cover: an exploratory analysis of <i>in situ</i> hyperspectral data. International Journal of Remote Sensing, 2009, 30, 6497-6517.	2.9	106
189	Generalization of Subpixel Analysis for Hyperspectral Data With Flexibility in Spectral Similarity Measures. IEEE Transactions on Geoscience and Remote Sensing, 2009, 47, 2165-2171.	6.3	53
190	Water use efficiency and evapotranspiration of winter wheat and its response to irrigation regime in the north China plain. Agricultural and Forest Meteorology, 2008, 148, 1848-1859.	4.8	136
191	Estimation of aboveground biomass using in situ hyperspectral measurements in five major grassland ecosystems on the Tibetan Plateau. Journal of Plant Ecology, 2008, 1, 247-257.	2.3	78
192	Land-use/land-cover change detection using change-vector analysis in posterior probability space. , 2008, , .		0
193	The spatial distribution patterns of biological soil crusts in the Gurbantunggut Desert, Northern Xinjiang, China. Journal of Arid Environments, 2007, 68, 599-610.	2.4	131
194	Sensitivity of the Enhanced Vegetation Index (EVI) and Normalized Difference Vegetation Index (NDVI) to Topographic Effects: A Case Study in High-density Cypress Forest. Sensors, 2007, 7, 2636-2651.	3.8	502
195	Correlation analysis of Normalized Different Vegetation Index (NDVI) difference series and climate variables in the Xilingole steppe, China from 1983 to 1999. Frontiers of Biology in China: Selected Publications From Chinese Universities, 2007, 2, 218-228.	0.2	8
196	Analysis of NDVI and scaled difference vegetation index retrievals of vegetation fraction. Remote Sensing of Environment, 2006, 101, 366-378.	11.0	449
197	Restoring urbanization process in China in the 1990s by using non-radiance-calibrated DMSP/OLS nighttime light imagery and statistical data. Science Bulletin, 2006, 51, 1614-1620.	1.7	141
198	The urbanization process of Bohai Rim in the 1990s by using DMSP/OLS data. Journal of Chinese Geography, 2006, 16, 174-182.	3.9	16

JIN CHEN

#	Article	IF	CITATIONS
199	A combined approach for estimating vegetation cover in urban/suburban environments from remotely sensed data. Computers and Geosciences, 2006, 32, 1299-1309.	4.2	23
200	Relating photosynthesis of biological soil crusts with reflectance: preliminary assessment based on a hydration experiment. International Journal of Remote Sensing, 2006, 27, 5393-5399.	2.9	14
201	A new index for mapping lichen-dominated biological soil crusts in desert areas. Remote Sensing of Environment, 2005, 96, 165-175.	11.0	99
202	Reagentless amperometric immunosensor for human chorionic gonadotrophin based on direct electrochemistry of horseradish peroxidase. Biosensors and Bioelectronics, 2005, 21, 330-336.	10.1	70
203	Developing land use scenario dynamics model by the integration of system dynamics model and cellular automata model. Science in China Series D: Earth Sciences, 2005, 48, 1979-1989.	0.9	78
204	Modelling scenarios of land use change in northern China in the next 50 years. Journal of Chinese Geography, 2005, 15, 177-186.	3.9	5
205	Estimation of regional net primary productivity (NPP) using a process-based ecosystem model: How important is the accuracy of climate data?. Ecological Modelling, 2004, 178, 371-388.	2.5	67
206	Evolving core-periphery interactions in a rapidly expanding urban landscape: The case of Beijing. Landscape Ecology, 2004, 19, 375-388.	4.2	36
207	A simple method for reconstructing a high-quality NDVI time-series data set based on the Savitzky–Golay filter. Remote Sensing of Environment, 2004, 91, 332-344.	11.0	1,679
208	Hyperspectral identification of grassland vegetation in Xilinhot, Inner Mongolia, China. International Journal of Remote Sensing, 2003, 24, 3171-3178.	2.9	29
209	An IHS-based change detection approach for assessment of urban expansion impact on arable land loss in China. International Journal of Remote Sensing, 2003, 24, 1353-1360.	2.9	22
210	Land-Use/Land-Cover Change Detection Using Improved Change-Vector Analysis. Photogrammetric Engineering and Remote Sensing, 2003, 69, 369-379.	0.6	278
211	Understanding of Natural Disaster Database Design and Compilation of Digital Atlas of Natural Disasters in China. Annals of GIS, 2000, 6, 153-158.	3.1	5
212	Zoning grassland protection area by using remote sensing and cellular automata model with a case study in Xilingol "typical steppe" grassland in Northern China. , 0, , .		1
213	Variability of the phenological stages of winter wheat in the North China Plain with NOAA/AVHRR NDVI data (1982-2000). , 0, , .		0
214	An effective approach to remove cloud-fog cover and enhance remotely sensed imagery. , 0, , .		1